

Variational Bayesian inversion for microwave breast imaging

Leila Gharsalli, H Ayasso, Bernard Duchêne, Ali Mohammad-Djafari

▶ **To cite this version:**

Leila Gharsalli, H Ayasso, Bernard Duchêne, Ali Mohammad-Djafari. Variational Bayesian inversion for microwave breast imaging. Computer Assisted Methods in Engineering and Science, 2014, 21 (3/4), pp.199-210. hal-01211734

HAL Id: hal-01211734

https://centralesupelec.hal.science/hal-01211734

Submitted on 5 Oct 2015

HAL is a multi-disciplinary open access archive for the deposit and dissemination of scientific research documents, whether they are published or not. The documents may come from teaching and research institutions in France or abroad, or from public or private research centers.

L'archive ouverte pluridisciplinaire **HAL**, est destinée au dépôt et à la diffusion de documents scientifiques de niveau recherche, publiés ou non, émanant des établissements d'enseignement et de recherche français ou étrangers, des laboratoires publics ou privés.

Computer Assisted Methods in Engineering and Science, **21**: 199–210, 2014.
Copyright © 2014 by Institute of Fundamental Technological Research, Polish Academy of Sciences

Variational Bayesian inversion for microwave breast imaging

Leila Gharsalli[1], Hacheme Ayasso[2], Bernard Duchêne[1], Ali Mohammad-Djafari[1]

[1] *Laboratoire des Signaux et Systèmes*
(L2S, UMR 8506: CNRS – Centrale-Supélec – Univ Paris-Sud)
3 rue Joliot-Curie, F-91190 Gif-sur-Yvette, France
e-mail: leila.gharsalli@lss.supelec.fr, bernard.duchene@lss.supelec.fr, ali.mohammad-djafari@lss.supelec.fr

[2] *Univ Grenoble-Alpes, GIPSA-Lab*
11 rue des mathématiques, Grenoble Campus, BP 46, F-38000 Grenoble, France
e-mail: hacheme.ayasso@gipsa-lab.fr

Microwave imaging is considered as a nonlinear inverse scattering problem and tackled in a Bayesian estimation framework. The object under test (a breast affected by a tumor) is assumed to be composed of compact regions made of a restricted number of different homogeneous materials. This *a priori* knowledge is defined by a Gauss-Markov-Potts distribution. First, we express the joint posterior of all the unknowns; then, we present in detail the variational Bayesian approximation used to compute the estimators and reconstruct both permittivity and conductivity maps. This approximation consists of the best separable probability law that approximates the true posterior distribution in the Kullback-Leibler sense. This leads to an implicit parametric optimization scheme which is solved iteratively. Some preliminary results, obtained by applying the proposed method to synthetic data, are presented and compared with those obtained by means of the classical contrast source inversion method.

Keywords: inverse scattering, microwave imaging, breast cancer detection, Gauss-Markov-Potts prior, variational Bayesian approximation.

1. Introduction

In the last few decades, microwave imaging has attracted an increasing interest in medical applications such as breast cancer detection [10, 12]. In addition to the non-ionizing nature of microwaves, one of the motivation for developing a microwave imaging technique for detecting breast cancer is the significant contrast in the dielectric properties at microwave frequencies of normal and malignant breast tissues [15]. All this makes microwave imaging a better alternative, in terms of cost and safety, than X-ray mammography which is the most widespread breast cancer detection technique.

Hence, measurements of the scattered fields resulting from the interaction between a known interrogating wave in the microwave frequency range and the breast can be used to find a contrast function that depends on the dielectric properties (permittivity and conductivity) of the breast. This leads to a non linear ill-posed inverse scattering problem solved herein in a variational Bayesian framework. The associated forward problem consists of modeling the wave-breast interaction through a domain integral representation of the electric field in a 2D configuration of a transverse magnetic polarization case.

The Bayesian framework [14] allows us to take easily into account prior information on the sought solution. Such prior information could consist of sparsity that represents, in the spectral domain,

the spatial correlation exhibited by constitutive properties of breast tissues as considered in [8] where microwave breast imaging is tackled by means of Bayesian inference applied to compressive sensing and efficient solutions are sought by means of the relevance vector machine technique [24]. Herein, we would like to call attention to the fact that the breast is composed of a finite number of different tissues distributed in compact regions. Indeed, it has been shown that although they are very heterogeneous and show large variability in their dielectric properties between individuals, the breast tissues can be divided into four different groups, three for healthy tissues [16], which are then classified with respect to their fat content, and one for cancerous tissues [18]. Then, in addition to retrieve a map of the contrast function, we would like to obtain a segmentation of the breast that differentiates these tissue groups. The sought image is then supposed to be composed of a finite number of homogeneous area and this *a priori* is introduced via a Gauss-Markov field with hidden Potts label fields [21].

Afterwards, the variational Bayesian approximation (VBA) [19] is applied to obtain an estimator of the unknowns. It can be noted that a semi-supervised context is considered herein as the number of different tissues is assumed to be known, while all the unknowns and other hyper-parameters of the model are estimated simultaneously through a joint posterior law. The purpose of VBA is to approximate the latter by a free-form distribution that minimizes the Kullback-Leibler divergence. This distribution is chosen as a separable law. Then, thanks to the latter method, the initial inverse problem turns into an optimization problem and an analytical approximation of the posterior is obtained. This method has already been applied to microwave imaging and optical diffraction tomography and the results have shown its improved performances with respect to computation time and simplicity, compared with stochastic sampling methods such as Markov chain Monte-Carlo (MCMC) [2, 3].

The main contribution of this work is the application of VBA to breast imaging where the sought contrast is complex valued, contrary to the case presented in [2], and both permittivity and conductivity maps have to be retrieved. Herein, we discuss the results obtained by means of this approach from synthetic data generated in different configurations involving two different numerical breast phantoms: a simple phantom made of two homogeneous media and a more sophisticated one made from a MRI scan of a real breast. Next, we present some results and compare with those obtained by means of the deterministic contrast source inversion method (CSI, [25, 26]).

This paper is organized as follows: Sec. 2 is about experimental configuration and forward modeling. The VBA approach and Bayesian computations are discussed in Sec. 3. In Sec. 4, the method is applied to synthetic data and compared to CSI. Finally, some conclusions and discussion are given in Sec. 5.

2. Forward modeling

2.1. Experimental configuration

We consider a 2D configuration in a transverse magnetic polarization case where the object under test is supposed to be cylindrical, with infinite extension along the z axis and illuminated by a line source whose location can be varied and that operates at several discrete frequencies. This source generates an incident electric field E^{inc} polarized along the z axis with an $\exp(-i\omega t)$ implicit time dependence and illuminates the breast from 64 various angular positions uniformly distributed around a 7.5-cm-radius circle centered at the origin and at 6 different frequencies in the range 0.5–3 GHz. For each frequency and illumination angle, 64 measurements of the scattered field are performed at angular positions uniformly distributed around the same circle. The breast is immersed in a background medium (domain $\mathcal{D}_1$) and is assumed to be contained in the test domain ($\mathcal{D}$). The different media are characterized by their propagation constant $k(\boldsymbol{r})$ such that $k^2(\boldsymbol{r}) = \omega^2\mu_0\epsilon_0\epsilon_r(\boldsymbol{r}) + i\omega\mu_0\sigma(\boldsymbol{r})$, where ω is the angular frequency, ϵ_0 and μ_0 are the permittivity and the permeability of the free space, respectively, $\boldsymbol{r} \in \mathcal{D}$ is an observation point and $\epsilon_r(\boldsymbol{r})$ and $\sigma(\boldsymbol{r})$ are respectively the relative permittivity and conductivity of the medium.

Two breast phantoms are considered (see Fig. 1). Both of them are assumed to be affected with a tumor (domain $\mathcal{D}_3$) with a 2-cm-diameter circular cross-section and with electromagnetic parameters $\epsilon_r = 55.3$ and $\sigma = 1.57$ Sm^{-1}. Phantom 1 is rather simple and it consists of a homogeneous breast (domain $\mathcal{D}_2$), with a 9.6-cm-diameter circular cross-section and relative dielectric permittivity and conductivity respectively equal to $\epsilon_r = 6.12$ and $\sigma = 0.11$ Sm^{-1}, immersed in a background medium of electromagnetic parameters $\epsilon_r = 10$ and $\sigma = 0.5$ Sm^{-1}. Phantom 2 is more sophisticated. It is made using a MRI scan of a real breast [27]. Hence, the breast is also assumed to be of circular cross-section with a diameter of 9.6 cm but it is now made of a very heterogeneous medium with parameters varying in the ranges $2.46 \leq \epsilon_r \leq 60.6$ and 0.01 Sm$^{-1} \leq \sigma \leq 2.28$ Sm^{-1}, surrounded by a 2-mm-thick skin with electromagnetic parameters $\epsilon_r = 35.7$ and $\sigma = 0.32$ Sm^{-1} and immersed in a background medium whose relative dielectric permittivity and conductivity are respectively equal to $\epsilon_r = 35$ and $\sigma = 0.5$ Sm^{-1}.

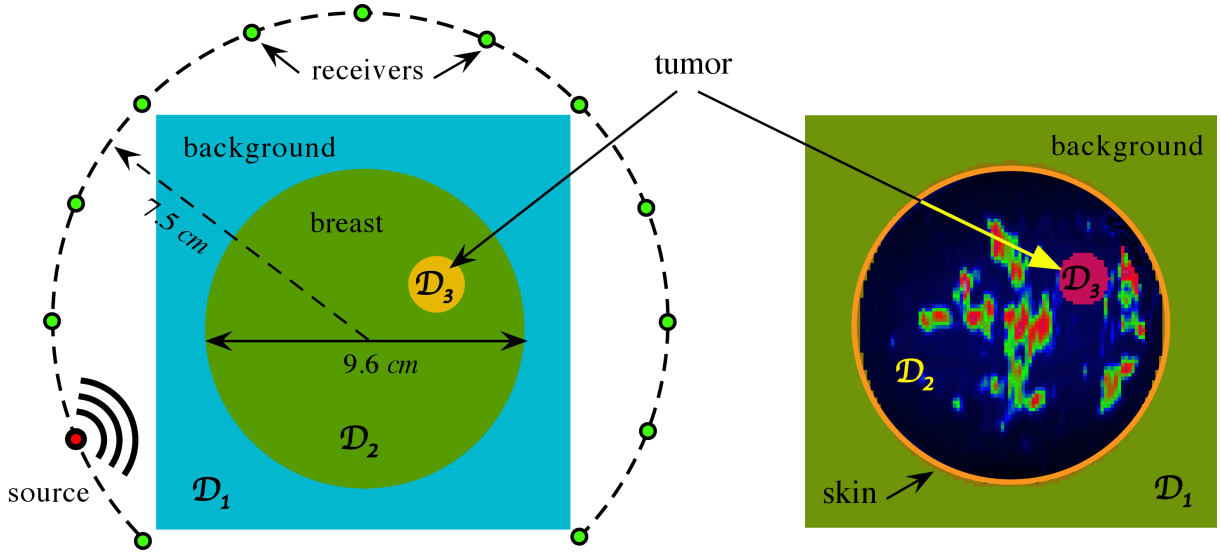


Fig. 1. Measurement configuration and breast phantoms (left: phantom 1, right: phantom 2).

2.2. Problem formulation

Modeling is based on a domain integral representation of the electric field obtained by applying Green's theorem to the Helmholtz wave equations satisfied by the fields and by accounting for continuity and radiation conditions [5]. The forward model consists of two coupled integral equations. The first one, denoted as the observation equation, is a Fredholm first kind integral equation that relates the scattered field observed on a measurement domain $\mathcal{S}$ to Huygens-type sources induced within the object by the incident wave, whereas the second one, denoted as the coupling (or state) equation, relates the total field inside the object to the induced sources [3, 7]. The forward problem is solved from discrete counterparts of these integral equations obtained by the method of moments with pulse basis and point matching [11], which results in partitioning the test domain $\mathcal{D}$ into $N_{\mathcal{D}}$ elementary pixels small enough to permit considering both the field and the contrast as constant over each of them. Let us now consider a contrast function χ, defined in $\mathcal{D}$ and null outside the object, such that $\chi(\boldsymbol{r}) = (k^2(\boldsymbol{r}) - k_1^2)/k_0^2$, where k_0 and k_1 are the propagation constants of free space and background medium, respectively. The Huygens-type sources $w(\boldsymbol{r})$ are then defined as $w(\boldsymbol{r}) = \chi(\boldsymbol{r})E(\boldsymbol{r})$, where $E(\boldsymbol{r})$ is the total field inside the object. The above-mentioned discrete counterparts then read:

$$\boldsymbol{y} = \boldsymbol{G}^o \boldsymbol{w} + \boldsymbol{\epsilon}, \tag{1}$$

$$\boldsymbol{w} = \boldsymbol{X}\boldsymbol{E}^{inc} + \boldsymbol{X}\boldsymbol{G}^c\, \boldsymbol{w} + \boldsymbol{\xi}, \tag{2}$$

where $\boldsymbol{y}$ is the vector containing the values of the scattered field $y(\boldsymbol{r})$ at the measurement points $\boldsymbol{r}$ ($\boldsymbol{r} \in \mathcal{S}$), $\boldsymbol{E}$, $\boldsymbol{\chi}$ and $\boldsymbol{w}$ are the vectors that contain the values of $E(\boldsymbol{r}')$, $\chi(\boldsymbol{r}')$ and $w(\boldsymbol{r}')$ at the centers $\boldsymbol{r}'$ of the pixels ($\boldsymbol{r}' \in \mathcal{D}$), $\boldsymbol{X}$ is a matrix such that $\boldsymbol{X} = \text{diag}(\boldsymbol{\chi})$, $\boldsymbol{G}^o$ and $\boldsymbol{G}^c$ are huge matrices whose elements result from the integration of the free space Green's function over the elementary pixels [3] and $\boldsymbol{\epsilon}$ and $\boldsymbol{\xi}$ are two vectors which account for model and measurement errors that are supposed to be centered, white and satisfying Gaussian laws (i.e., $\boldsymbol{\epsilon} \sim \mathcal{N}(\boldsymbol{0}, v_\epsilon \mathbf{I})$ and $\boldsymbol{\xi} \sim \mathcal{N}(\boldsymbol{0}, v_\xi \mathbf{I})$).

2.3. Validation of the forward model

First, in the forward problem we solve Eq. (2) for the induced sources $\boldsymbol{w}$, knowing the contrast $\boldsymbol{\chi}$ and the incident field $\boldsymbol{E}^{inc}$, and then we solve Eq. (1) for the scattered field $\boldsymbol{y}$. At this point it can be noted that this direct model is used in the inversion. However, in order to avoid committing an inverse crime in the sense of [6] which would consist of testing the inversion algorithm on data obtained by means of a model closely related to that used in inversion, the synthetic data of the inverse problem are computed in a different way, by benefiting from the circular symmetry that exists in the absence of inhomogeneities. Hence, the data are computed by means of a model (the data model) where discretization applies only to the domain $\mathcal{D}_3$ occupied by the tumor for both phantoms and to a part of the domain $\mathcal{D}_2$ for phantom 2, whereas the breast, the skin and the background medium are considered as cylindrically stratified embedding medium and the Green's function is modified consequently [23]. Figure 2 displays the scattered fields obtained by means of the data model with phantom 1 for the illumination angle of 45° and at two operating frequencies

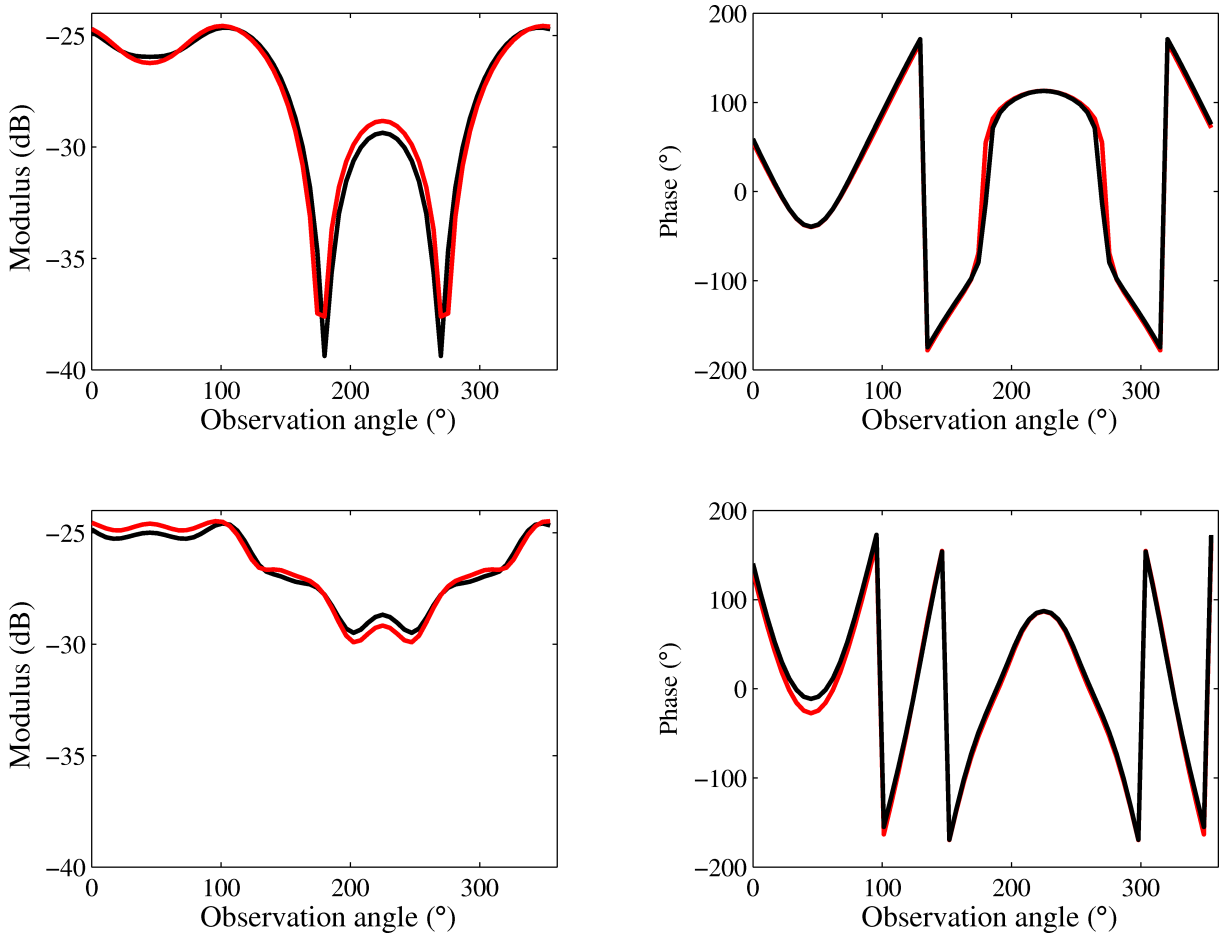


Fig. 2. Amplitude (left) and phase (right) of the scattered fields computed by means of the data model (black line) and by means of the forward model used for inversion (red line) at 1.5 GHz (top) and 3 GHz (bottom).

(1.5 GHz and 3 GHz), compared with that obtained by means of the forward model used for inversion where the test domain $\mathcal{D}$ is a square with 12.16 cm side partitioned into 64×64 square pixels each with a side $\delta = 1.9$ mm. It can be observed that the results fit relatively well.

3. Bayesian inversion approach

3.1. Hierarchical prior model

The inverse problem consists of retrieving the unknown contrast $\boldsymbol{\chi}$, or more precisely the relative permittivity ϵ_r and the conductivity σ, from the scattered field $\boldsymbol{y}$, given the incident field $\boldsymbol{E}^{inc}$. As the induced sources $\boldsymbol{w}$ are also unknown, they must be obtained at the same time as $\boldsymbol{\chi}$. Hence, assuming that their relation to the contrast is given by the state Eq. (2), we define their conditional *a priori* probability law as:

$$p(\boldsymbol{w}|\boldsymbol{\chi}, v_\xi) \propto \exp\left\{-\frac{1}{2v_\xi}||\boldsymbol{w} - \boldsymbol{X}\boldsymbol{E}^{inc} - \boldsymbol{X}\boldsymbol{G}^c\boldsymbol{w}||^2_{\mathcal{D}}\right\}. \tag{3}$$

In the same way, the observation Eq. (1) yields the conditional *a priori* probability law for the scattered field:

$$p(\boldsymbol{y}|\boldsymbol{w}, v_\epsilon) \propto \exp\left\{-\frac{1}{2v_\epsilon}||\boldsymbol{y} - \boldsymbol{G}^o\boldsymbol{w}||^2_{\mathcal{S}}\right\}. \tag{4}$$

Now, let us introduce *a priori* information for the sought solution required in order to counteract the ill-posedness of the inverse problem. It consists of the fact that the sought object is composed of a restricted number K of homogeneous materials distributed in compact regions. The compactness of the different regions can be accounted for by means of a hidden variable (or classification label) $z(\boldsymbol{r})$ associated with each pixel $\boldsymbol{r}$, which represents a segmentation of the unknown object. The classification label $z(\boldsymbol{r})$ of a pixel $\boldsymbol{r}$ is related, in a probabilistic way, to that of its neighbors by means of a Potts-Markov model for $\boldsymbol{z}$:

$$p(\boldsymbol{z}|\lambda) = \frac{1}{T(\lambda)} \exp\left\{\lambda \sum_{\boldsymbol{r}\in\mathcal{D}} \sum_{\boldsymbol{r}'\in\mathcal{V}_{\boldsymbol{r}}} \delta\left(z(\boldsymbol{r}) - z(\boldsymbol{r}')\right)\right\}, \tag{5}$$

where λ is the Potts parameter that determines the correlation between neighbors, $T(\lambda)$ is a normalization factor and $\mathcal{V}_{\boldsymbol{r}}$ is a neighborhood of $\boldsymbol{r}$, herein made of the four nearest pixels. It can be noted that the value of λ determines the *a priori* behavior of the hidden field and hence the size of the homogeneous area in the final image; the larger λ is, the larger the area is. Herein, it is set to $\lambda = 1$, i.e., to a value slightly higher than the critical value $\lambda_c = \log(1 + \sqrt{K})$, which yields a good tradeoff for the degree of correlation [4]. In this way the number of homogeneous areas remains reasonably low while small details of high contrast such as those that appear in phantom 2, are relatively well preserved.

The fact that the breast is composed of a finite number of different tissues can then be expressed by the following conditional distribution:

$$p(\chi(\boldsymbol{r})|z(\boldsymbol{r}) = k) = \mathcal{N}(m_k, v_k), \qquad k = 1, \ldots, K, \tag{6}$$

which means that all the pixels with the same label ($z(\boldsymbol{r}) = k$, $k \in \{1, ..., K\}$) correspond to the same tissue whose contrast satisfies the Gaussian law with a mean value m_k and a variance v_k. Hence, the contrast is sought as a Gaussian mixture where each Gaussian law represents a given tissue and its values belong to a continuous set. Let us emphasize the fact that two *a priori* models can now be defined, depending on the way in which the means m_k and variances v_k are estimated. With the first model, denoted as independent Gaussian mixture (IGM), the interaction between

pixels is accounted for only through the hidden field $z(\boldsymbol{r})$ while the contrasts of the pixels of a given region are conditionally independent, and the mean m_k and variance v_k depend only on the class k. On the contrary, the second model, denoted as Gauss-Markov mixture (GMM), reinforces the correlation between pixels of the same class through a Markov field, while keeping independent the pixels of the other classes in order to preserve the contours. This is done by setting the *a priori* mean of the contrast of a pixel to the mean of the contrast of its nearest neighbors if they are in the same class, or to the mean of the class otherwise. The latter model is more suitable when the sought object is very heterogeneous.

Now we have all the components necessary to find the expression of the joint posterior law of all the unknowns ($\boldsymbol{\chi}$, $\boldsymbol{w}$, $\boldsymbol{z}$, $\boldsymbol{\psi}$), where $\boldsymbol{\psi}$ is the set of hyper-parameters of the model ($\boldsymbol{\psi} = \{\boldsymbol{m}, \boldsymbol{v}, v_\epsilon, v_\xi\}$). This posterior law is obtained by applying the Bayes formula:

$$\begin{aligned} p(\boldsymbol{\chi}, \boldsymbol{w}, \boldsymbol{z}, \boldsymbol{\psi}|\boldsymbol{y}) \propto p(\boldsymbol{y}|\boldsymbol{w}, v_\epsilon)\, p(\boldsymbol{w}|\boldsymbol{\chi}, v_\xi)\, p(\boldsymbol{\chi}|\boldsymbol{z}, \boldsymbol{m}, \boldsymbol{v}) p(\boldsymbol{z}|\lambda) \\ \times p(m_k|\mu_0, \tau_0)\, p(v_k|\eta_0, \phi_0)\, p(v_\epsilon|\eta_\epsilon, \phi_\epsilon)\, p(v_\xi|\eta_\xi, \phi_\xi). \end{aligned} \tag{7}$$

Expressions of $p(\boldsymbol{y}|\boldsymbol{w}, v_\epsilon)$, $p(\boldsymbol{w}|\boldsymbol{\chi}, v_\xi)$, $p\,(\boldsymbol{\chi}|\boldsymbol{z}, \boldsymbol{m}, \boldsymbol{v})$ and $p(\boldsymbol{z}|\lambda)$ are derived respectively from Eqs. (3)–(6). As for the hyper-parameters, they are assumed to satisfy conjugate prior laws so that the posterior laws stay in the same family, which greatly simplifies the computations. Hence, Gaussian ($\mathcal{N}(\mu, \tau)$) and inverse-gamma ($\mathcal{IG}(\eta, \phi)$) distributions are assigned to means and variances, respectively:

$$\begin{aligned} &p(m_k|\mu_0, \tau_0) = \mathcal{N}(\mu_0, \tau_0), \qquad && p(v_k|\eta_0, \phi_0) = \mathcal{IG}(\eta_0, \phi_0), \\ &p(v_\epsilon|\eta_\epsilon, \phi_\epsilon) = \mathcal{IG}(\eta_\epsilon, \phi_\epsilon), \qquad && p(v_\xi|\eta_\xi, \phi_\xi) = \mathcal{IG}(\eta_\xi, \phi_\xi), \end{aligned} \tag{8}$$

where μ_0, τ_0, η_0, ϕ_0, η_ϵ, ϕ_ϵ, η_ξ and ϕ_ξ are meta-hyper-parameters appropriately set to have non-informative priors, i.e. flat prior distributions.

3.2. The variational Bayesian approach

All the right-hand side expressions of Eq. (8) are known, which allows us to obtain the expression of the left-hand side, i.e., the joint posterior law of all the unknowns, up to a normalizing constant. However, the complexity of its expression makes it very hard to obtain it in a tractable form for conventional estimators, such as the maximum *a posteriori* (MAP) or the posterior mean (PM), and thus an approximation is required. Hence, we opt for an analytical approximation based on the variational Bayesian approach (VBA, [22]) that aims to approximate the true posterior distribution (8) by a free-form separable law $q(\boldsymbol{u}) = \prod_j q(\boldsymbol{x}_j)$, with $\boldsymbol{u} = \{\boldsymbol{\chi}, \boldsymbol{w}, \boldsymbol{z}, \boldsymbol{\psi}\}$, that minimizes the Kullback-Leibler divergence $\mathrm{KL}(q||p) = \int q \ln(q/p)$ [13]. We define the separable law as

$$q(\boldsymbol{u}) = q(v_\epsilon) q(v_\xi) \prod_{i=1}^{N_\mathcal{D}} q(\chi_i) q(w_i) q(z_i) \prod_{k=1}^{K} q(m_k) q(v_k). \tag{9}$$

Then, we look for the optimal form of q that minimizes the Kullback divergence. This leads to the following parametric distributions:

$$\begin{aligned} &q(\boldsymbol{w}) = \mathcal{N}(\widetilde{\boldsymbol{m}}_w, \widetilde{\boldsymbol{V}}_w), \qquad q(\boldsymbol{\chi}) = \mathcal{N}(\widetilde{\boldsymbol{m}}_\chi, \widetilde{\boldsymbol{V}}_\chi), \qquad q(\boldsymbol{z}) = \prod_{\boldsymbol{r}} \widetilde{\boldsymbol{\zeta}}_k(\boldsymbol{r}), \\ &q(m_k) = \mathcal{N}(\widetilde{\mu}_k, \widetilde{\tau}_k), \qquad q(v_k) = \mathcal{IG}(\widetilde{\eta}_k, \widetilde{\phi}_k), \qquad q(v_\epsilon) = \mathcal{IG}(\widetilde{\eta}_\epsilon, \widetilde{\phi}_\epsilon), \qquad q(v_\xi) = \mathcal{IG}(\widetilde{\eta}_\xi, \widetilde{\phi}_\xi), \end{aligned} \tag{10}$$

where the tilded variables are mutually dependent and are computed in an iterative way [2] and, in the approximating law $\prod_{\boldsymbol{r}} \widetilde{\boldsymbol{\zeta}}_k(\boldsymbol{r})$, the probability of the hidden field of a pixel is computed from the probabilities of its neighbors at the previous iteration step.

3.3. Initialization and convergence of the algorithm

The initial number of classes K used for segmentation is set to $K = 3$ for phantom 1 and $K = 4$ for phantom 2, whereas the initial values $\boldsymbol{\chi}^{(0)}$ and $\boldsymbol{w}^{(0)}$ are obtained by backpropagating the scattered field data from the measurement circle $\mathcal{S}$ onto the test domain $\mathcal{D}$ [25]. From $\boldsymbol{\chi}^{(0)}$ and $\boldsymbol{w}^{(0)}$, the classification $\boldsymbol{z}$ and the hyper-parameters (means and variances) can be initialized by means of *K-means* clustering [20]. Here, given the fact that the contrast is complex valued, first the real part is segmented and the same segmentation is then used to initialize the imaginary part.

Concerning the convergence, the shaping parameters of Eq. (10) are iterated until convergence is reached. The latter is estimated empirically by studying the development of contrast and hyper-parameters in the course of iterations (see Fig. 3).

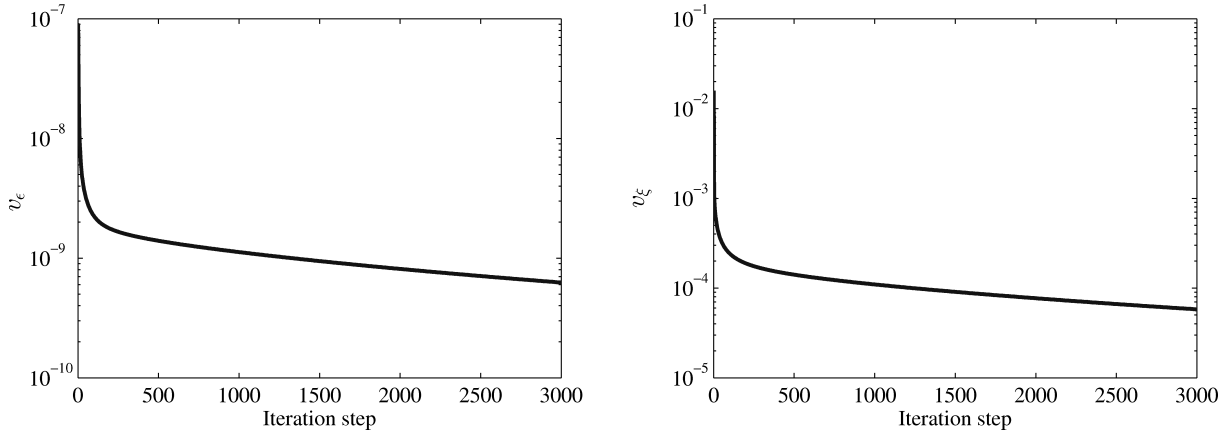


Fig. 3. The evolution of the observation v_ϵ (left) and coupling v_ξ (right) error variances as functions of the iteration step for phantom 1.

Finally, the efficiency of the various algorithms is estimated by means of the relative error (Err) or the peak signal to noise ratio (PSNR):

$$\mathrm{Err} = \frac{\sum\limits_{i=1}^{N_\mathcal{D}} \left(\gamma(\boldsymbol{r}_i) - \gamma_a(\boldsymbol{r}_i)\right)^2}{\sum\limits_{i=1}^{N_\mathcal{D}} \left(\gamma_a(\boldsymbol{r}_i)\right)^2}, \qquad \mathrm{PSNR\,(dB)} = 10 \log_{10} \left(\frac{N_\mathcal{D} \left|\chi_{\max}\right|^2}{\sum\limits_{i=1}^{N_\mathcal{D}} \left|\chi(\boldsymbol{r}_i) - \chi_a(\boldsymbol{r}_i)\right|^2} \right), \tag{11}$$

where $\gamma = \epsilon_r$ or σ, subscript a stands for the actual value and $\chi_{\max}$ is the maximal value of the contrast modulus.

4. Results

Figure 4 displays the results obtained for both permittivity and conductivity of phantom 1 after 500 iterations, in a test domain $\mathcal{D}$ partitioned into 64×64 square pixels, each with a side of 1.9 mm, while Fig. 5 displays those obtained for phantom 2 after 2000 iterations, in the test domain $\mathcal{D}$ partitioned into 120×120 square pixels, each with a side of 1 mm. These results are obtained by simultaneously processing the data corresponding to all frequencies and all directions of illumination. They are compared with those obtained by means of contrast source inversion (CSI, [25, 26]) under the same conditions and after the same number of iterations. The latter is an iterative deterministic method which consists of minimizing a cost functional, that accounts for both observation and coupling equations, by alternately updating $\boldsymbol{w}$ and $\boldsymbol{\chi}$ with a gradient-based method. In general, VBA succeeds in retrieving homogeneous regions that correspond to the background, the breast and the tumor and the results are more accurate than those obtained by means of CSI, particularly

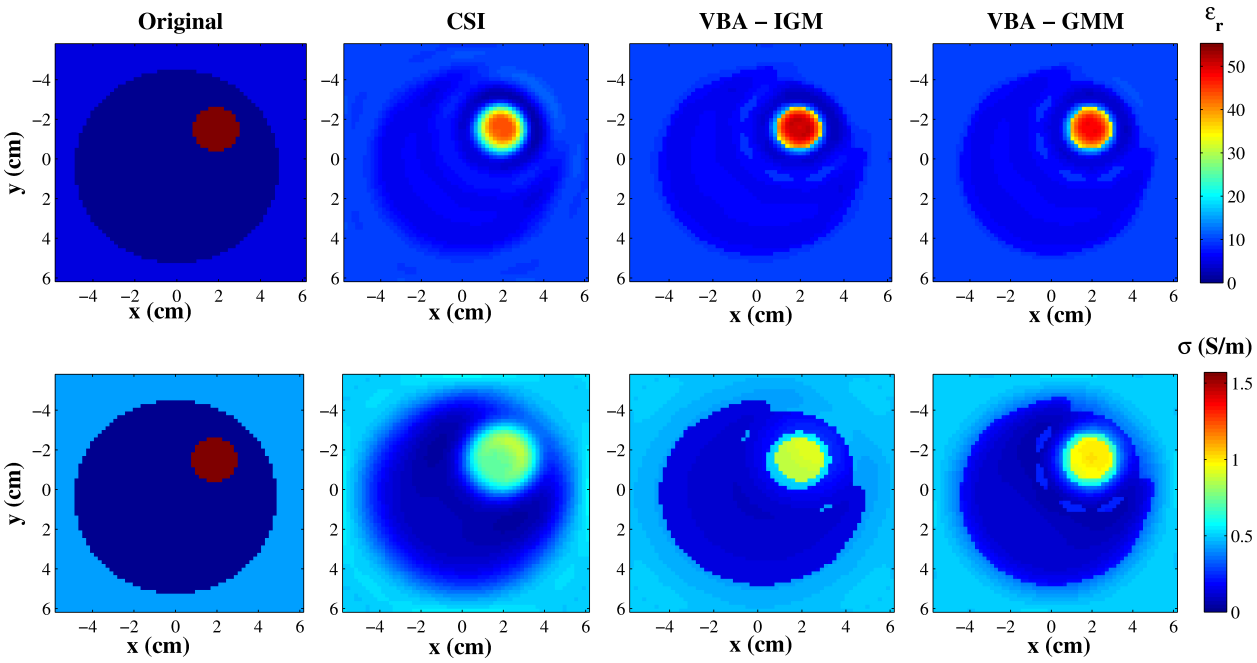


Fig. 4. Maps of permittivity (top row) and conductivity (bottom row) of phantom 1 reconstructed by means of CSI (2nd column) and VBA with the IGM (3rd column) and GMM (4th column) *a priori* models compared with the actual object (1st column).

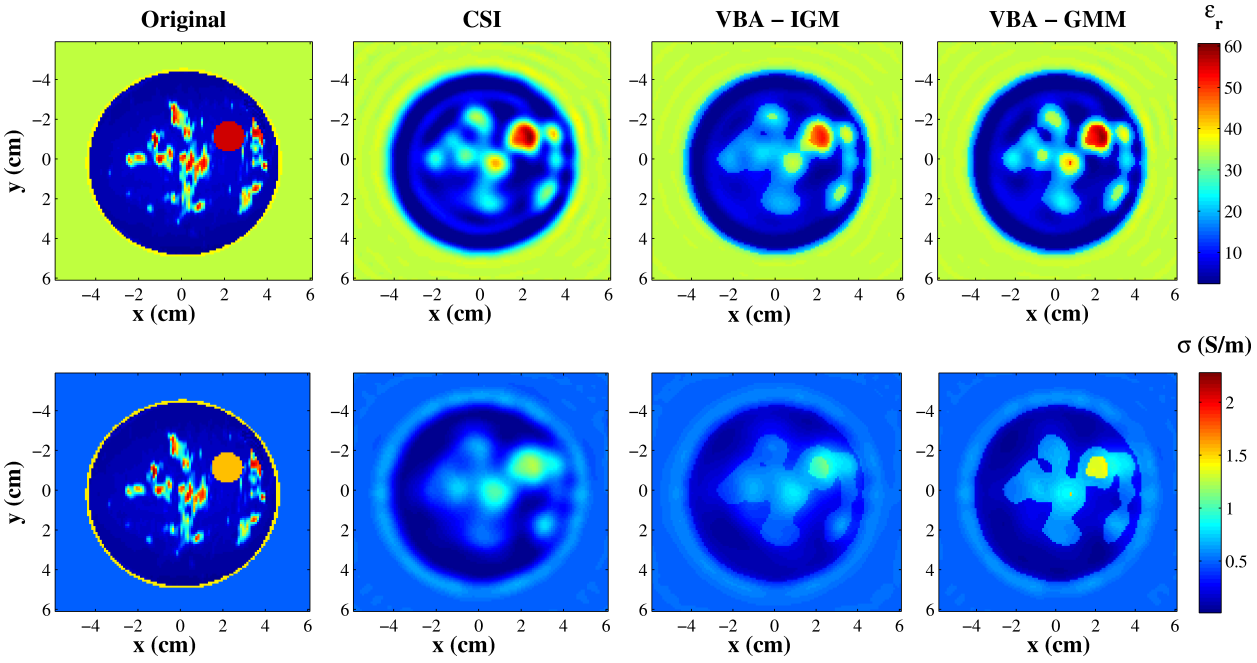


Fig. 5. Maps of permittivity (top row) and conductivity (bottom row) of phantom 2 reconstructed by means of CSI (2nd column) and VBA with the IGM (3rd column) and GMM (4th column) *a priori* models compared with the actual object (1st column).

concerning the conductivity. It can be noted that, for both phantoms, the GMM *a priori* model performs better in retrieving the tumor than the IGM one, which is, here again, more apparent in the conductivity maps than in the permittivity ones. This is confirmed in Table 1 that displays the PSNRs obtained for both phantoms with each of the methods. However, none of the *a priori* models succeeds in retrieving the glandular areas present in phantom 2, which is not surprising as these area do not correspond to compact homogeneous regions.

Table 1. PSNRs (dB) obtained for both phantoms with CSI, VBA-IGM and VBA-GMM.

Phantom	CSI	VBA	
		IGM	GMM
1	49.14	50.67	50.80
2	52.06	52.91	54.04

Finally, in addition to its better performances, the VBA compared with CSI yields not only an image of the sought object, but also a segmentation of the latter and an estimate of the various hyper-parameters as illustrated in Fig. 6.

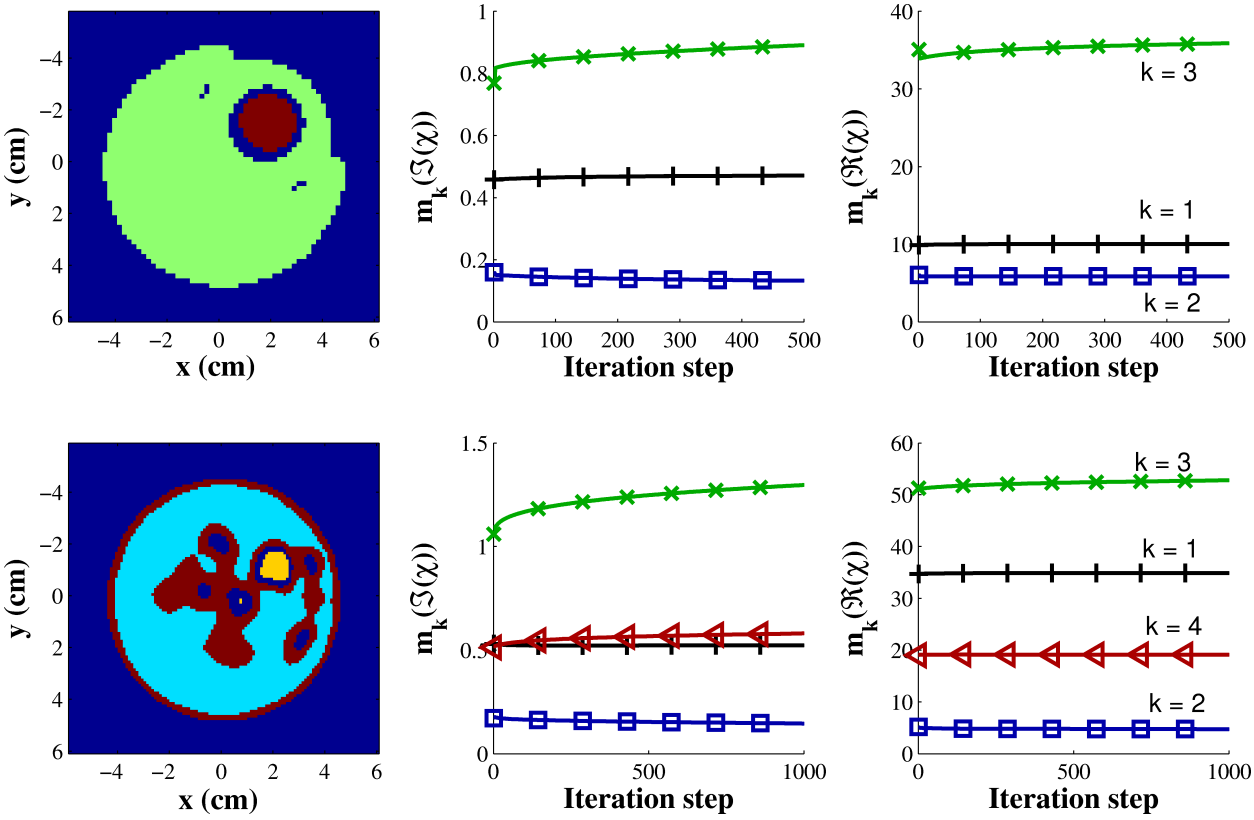


Fig. 6. Hidden fields (left) and means m_k of the real (right) and imaginary (middle) parts of the contrast corresponding to different classes for phantoms 1 (top row) and 2 (bottom row).

As underlined previously, a model error is systematically introduced when computing the synthetic data of the inverse problem. However, this does not account for measurement noise that would be inevitably present in real experimental situations. In order to test the sensitivity of VBA with respect to the latter, the data sets corresponding to both phantoms have been corrupted by additive white Gaussian noises, with signal to noise ratios (SNRs) equal to 5 dB, 10 dB and 20 dB, defined with respect to the scattered fields. It can be observed that the VBA is a very robust method that still succeeds in identifying the area corresponding to the tumor with SNR as low as 5 dB (see Figs. 7 and 8). Table 2 summarizes relative errors obtained for the relative permittivity and conductivity of both phantoms with various SNRs.

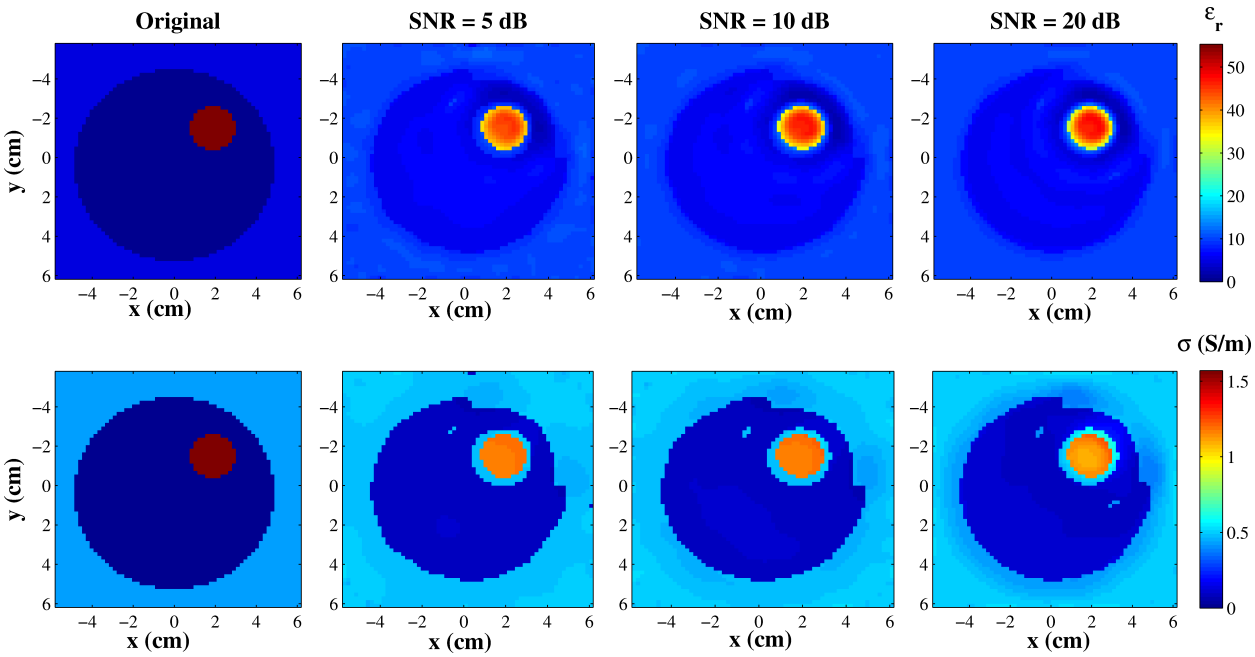


Fig. 7. Permittivity (top row) and conductivity (bottom row) maps of phantom 1 obtained from noisy data.

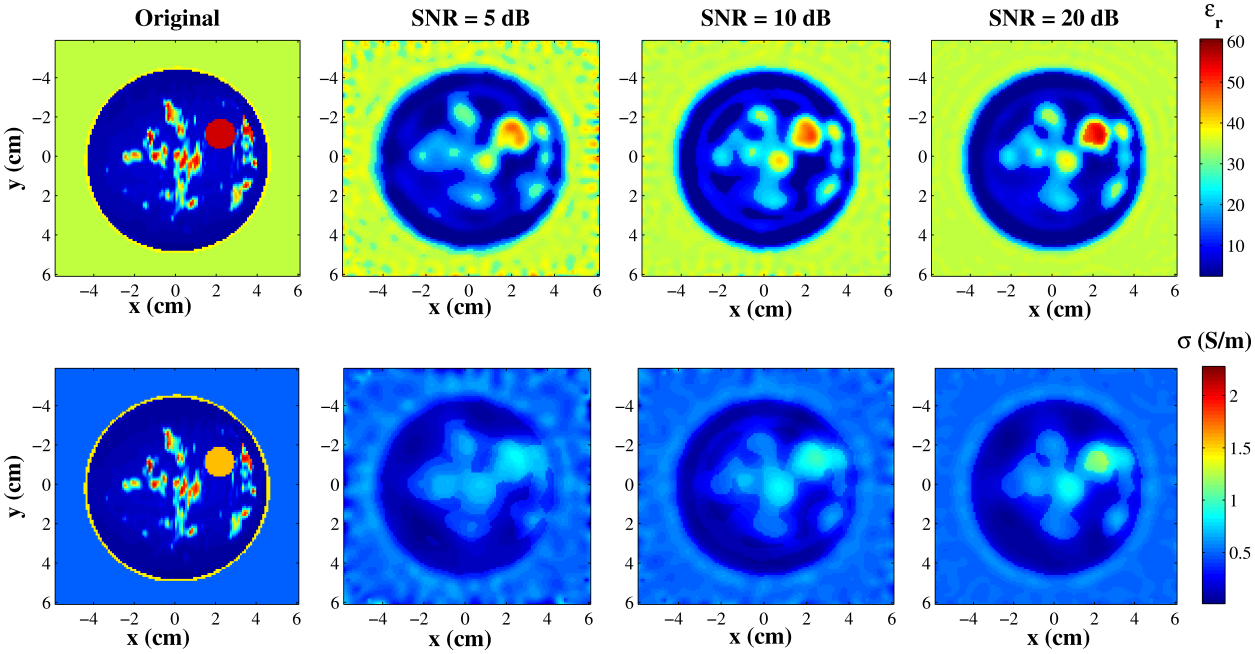


Fig. 8. Permittivity (top row) and conductivity (bottom row) maps of phantom 2 obtained from noisy data.

Table 2. Relative errors (Err) obtained for both phantoms with various SNRs.

SNR [dB]	Phantom 1		Phantom 2	
	ϵ_r	σ	ϵ_r	σ
5	0.2×10^{-2}	7.2×10^{-2}	2.5×10^{-1}	7.8×10^{-2}
10	0.8×10^{-5}	0.7×10^{-2}	2.4×10^{-3}	0.9×10^{-2}
20	2.6×10^{-9}	0.9×10^{-4}	3.4×10^{-4}	1.5×10^{-4}

5. Conclusion

In this paper, we consider microwave imaging as an inverse obstacle scattering problem which is known to be ill-posed. This means that a regularization of the problem is required prior to its resolution, and this regularization generally consists of introducing *a priori* information for the sought solution. Herein, an important information about the object under test is that it is composed of a restricted number of homogeneous materials distributed in compact regions. This is tackled in a Bayesian inversion framework via a Gauss-Markov-Potts model. Application to synthetic data shows a good improvement in the reconstruction quality with respect to a CSI deterministic approach. Moreover, compared with the latter, the Bayesian inversion has the advantage of providing not only the map of the contrast of the sought object, but also its segmentation into homogeneous regions and contrast parameters (means and variances) in each of the latter, in addition to the variances of the measurement and model errors and different hyper-parameters involved in the model. However, several points still need to be investigated. Particularly, concerning the convergence speed, a gradient-like variational Bayesian method [9] needs further research. This technique had already shown its effectiveness compared with the classical VBA in other applications. Another point under investigation is concerning the number of classes; herein, it is considered as *a priori* known, which is not necessarily true. If the latter is unknown, it can be determined by means of a non-parametric approach or it can be initialized at high level. In the latter case, it has been numerically shown [1] that it should converge to the optimal number of classes in one of two possible ways: i) if the number of pixels that belong to a given class decreases during iterations and reaches a low threshold value, then this class should disappear and ii) if the means of two different classes are close enough to one another, then these classes end up merging. Finally, concerning the physics of the application, it has been regarded in this paper that the dielectric properties of breast tissues do not change versus frequency, however they are very dispersive and it has been shown that the frequency behavior of the properties of the various tissue groups can be described by one-pole Debye models [17]. Hence, the next step is to account for the tissue frequency dispersivity by looking for the invariant parameters of the Debye models instead of the permittivity and conductivity of various tissue groups.

Acknowledgment

The authors would like to acknowledge E. Zastrow, S.K. Davis, M. Lazebnik, F. Kelcz, B.D. Van Veem and S.C. Hagness for the numerical model of breast phantom 2.

References

[1] H. Ayasso. *Une approche bayésienne de l'inversion. Application à l'imagerie de diffraction dans les domaines micro-onde et optique*. Ph.D. thesis, Université Paris-Sud 11, 2010.

[2] H. Ayasso, B. Duchêne, A. Mohammad-Djafari. Optical diffraction tomography within a variational Bayesian framework. *Inverse Problems in Science and Engineering*, **20**(1): 59–73, 2012.

[3] H. Ayasso, B. Duchêne, A. Mohammad-Djafari. MCMC and variational approaches for Bayesian inversion in diffraction imaging. In: J.-F. Giovannelli, J. Idier [Eds.], *Regularization and Bayesian Methods for Inverse Problems in Signal and Image Processing*, 201–224, Wiley-ISTE, 2015.

[4] V. Beffara, H. Duminil-Copin. The self-dual point of the two-dimensional random-cluster model is critical for $q \geq 1$. *Probability Theory and Related Fields*, **153**(3–4): 511–542, 2012.

[5] W.C. Chew. *Waves and fields in inhomogeneous media*. IEEE Press, New York, 1995.

[6] D. Colton, R. Kress. *Inverse acoustic and electromagnetic scattering theory*. Springer, New York, 1992.

[7] O. Féron, B. Duchêne, A. Mohammad-Djafari. Microwave imaging of inhomogeneous objects made of a finite number of dielectric and conductive materials from experimental data. *Inverse Problems*, **21**(6): S95–S115, 2005.

[8] A.E. Fouda, F.L. Teixeira. Ultra-wideband microwave imaging of breast cancer tumors via Bayesian inverse scattering. *Journal of Applied Physics*, **115**(6): 064701, 2014.

[9] A. Fraysse, T. Rodet. A measure-theoretic variational Bayesian algorithm for large dimensional problems. *SIAM Journal on Imaging Sciences*, **7**(4): 2591–2622, 2014.

[10] S.C. Hagness, E.C. Fear, A. Massa. Guest editorial: special cluster on microwave medical imaging. *IEEE Antennas and Wireless Propagation Letters*, **11**: 1592–1597, 2012.
[11] R.F. Harrington. *Field computation by moment methods*. The Macmillan Company, New York, 1968.
[12] A.M. Hassan, M. El-Shenawee. Review of electromagnetic techniques for breast cancer detection. *IEEE Reviews in Biomedical Engineering*, **4**: 103–118, 2011.
[13] G.E. Hinton, D. van Camp. Keeping the neural networks simple by minimizing the description length of the weights. In: L. Pitt [Ed.], *Proceedings of the 6th Annual Conference on Computational Learning Theory*, 5–13, ACM, New York, 1993.
[14] J. Idier [Ed.]. *Bayesian approach to inverse problems*. Wiley-ISTE, 2008.
[15] W.T. Joines, R.L. Jirtle, M.D. Rafal, D.J. Schaefer. Microwave power absorption differences between normal and malignant tissue. *International Journal of Radiation Oncology • Biology • Physics*, **6**(6): 681–687, 1980.
[16] M. Lazebnik, L. McCartney, D. Popovic, C.B. Watkins, M.J. Lindstrom, J. Harter, S. Sewall, A. Magliocco, J.H. Booske, M. Okoniewski, S.C. Hagness. A large-scale study of the ultrawideband microwave dielectric properties of normal breast tissue obtained from reduction surgeries. *Physics in Medicine and Biology*, **52**(10): 2637–2656, 2007.
[17] M. Lazebnik, M. Okoniewski, J.H. Booske, S.C. Hagness. Highly accurate Debye models for normal and malignant breast tissue dielectric properties at microwave frequencies. *IEEE Microwave and Wireless Components Letters*, **17**(12): 822–824, 2007.
[18] M. Lazebnik, D. Popovic, L. McCartney, C.B. Watkins, M.J. Lindstrom, J. Harter, S. Sewall, T. Ogilvie, A. Magliocco, T.M. Breslin, W. Temple, D. Mew, J.H. Booske, M. Okoniewski, S.C. Hagness. A large-scale study of the ultrawideband microwave dielectric properties of normal, benign, and malignant breast tissues obtained from cancer surgeries. *Physics in Medicine and Biology*, **52**(20): 6093–6115, 2007.
[19] D.J.C. Mackay. *Information theory, inference, and learning algorithms*. Cambridge University Press, Cambridge, 2003.
[20] J.B. MacQueen. Some methods for classification and analysis of multivariate observations. In: *Proceedings of the 5th Berkeley Symposium on Mathematical Statistics and Probability*, University of California Press, **1**: 281–297, 1967.
[21] A. Mohammad-Djafari. Gauss-Markov-Potts priors for images in computer tomography resulting to joint optimal reconstruction and segmentation. *International Journal of Tomography and Statistics*, **11**: 76–92, 2008.
[22] V. Smídl, A. Quinn. *The variational Bayes method in signal processing*. Springer Verlag, Berlin, 2006.
[23] C-T. Tai. *Dyadic green functions in electromagnetic theory*. IEEE Press, New York, 1993.
[24] M.E. Tipping. Sparse Bayesian learning and the relevance vector machine. *The Journal of Machine Learning Research*, **1**: 211–244, 2001.
[25] P.M. van den Berg, R.E. Kleinman. A contrast source inversion method. *Inverse Problems*, **13**(6): 1607–1620, 1997.
[26] P.M. van den Berg, A. van Broekhoven, A. Abubakar. Extended contrast source inversion. *Inverse Problems*, **15**(5): 1325–1344, 1999.
[27] E. Zastrow, S.K. Davis, M. Lazebnik, F. Kelcz, B.D. Van Veem, S.C. Hagness. *Database of 3D grid-based numerical breast phantoms for use in computational electromagnetics simulations*. University of Wisconsin-Madison, Online, 2008.